Applied Acoustics 130 (2018) 230–237

Contents lists available at ScienceDirect

Applied Acoustics

journal homepage: www.elsevier.com/locate/apacoust

The accuracy of some models for the airflow resistivity of nonwoven materials

A.I. Hurrell[a,*], K.V. Horoshenkov[a], M.T. Pelegrinis[b]

[a] Department of Mechanical Engineering, The University of Sheffield, Sheffield S1 3JD, United Kingdom
[b] John Cotton Group Ltd, Nunbrook Mills, Huddersfield Road, Mirfield WF14 0EH, United Kingdom

ARTICLE INFO

Keywords:
Airflow
Resistivity
Nonwoven
Inversion
Fibrous
Impedance

ABSTRACT

The airflow resistivity is a key parameter to consider when evaluating the acoustic performance of a fibrous material. The airflow resistivity is directly linked to a fibrous materials acoustic properties which allows for the non-invasive measurements of the fibre diameter and material density from acoustical data. There are several models that relate the airflow resistivity to the acoustic behaviour through the material's density and fibre diameter. It is not always obvious how accurately a model represents the true value of the flow resistivity of a nonwoven material with a fibre size variation. Therefore, the scope of this paper is to compare the performance of several theoretical and empirical models applied to a representative range of nonwoven fibrous media composed of blends of different fibre sizes and types. Being able to understand the performance of these models in application to fibre blends will enable users to characterise these types of fibrous media more precisely. From this work, it was concluded that the Miki model (Miki, 1990) is the most accurate model to invert the airflow resistivity from acoustical surface impedance of a wide range of nonwoven blends.

1. Introduction

Airflow resistivity is an important parameter when considering the acoustic performance of a material. There have been several studies looking into this area since the original work conducted by Nichols [1], which proposed a relation between this parameter and the fibre diameter and density of a material. The realisation that airflow resistivity is directly linked to the acoustic properties of fibrous media allows for the measurement of both fibre diameter and material density rapidly and non-invasively from acoustical data, such as the surface impedance or absorption coefficient [2,3]. One question this paper addresses is how well a model can invert these parameters from a standard acoustic impedance tube test [4] performed on a nonwoven fibrous blend specimen? Another question this paper addresses is how accurate are some models which relate the fibre diameter, density and flow resistivity. To answer the first question, this paper aims to study the performance of two models used to predict the acoustical properties of fibrous media and compare the inversion results against measured and predicted flow resistivity data. To answer the second question, this paper studies the performance of three popular models which predict the flow resistivity from the material microstructure and density data. The understanding of the accuracy of these models is useful to develop new efficient fibrous products for a broad range of acoustic absorption applications and to appreciate their limitations when used for material parameter inversion.

In order to compare these models, a representative range of nonwoven fibrous media was provided by John Cotton Group Ltd. These media were composed of fibres of variable diameters and varied in density, thickness, porosity, and pore composition. A thermosetting binder fibre was also added to the blend, which, when heated, partially melts and so fixes the layers of fibres in place. Such variations were used to ascertain if there are any models which are more suited to certain types of fibrous media or if there is a model to be found which performs particularly well across all types of nonwoven fibrous media.

The paper is organised in the following manner. Section 2 presents the models which were used to predict the flow resistivity from fibre and density information or to invert it from acoustical data. Section 3 presents the experimental methodology which was used to measure acoustical and related non-acoustical characteristics of fibrous media. Sections 4 and 5 are the discussion and conclusions, respectively.

2. Model introduction

Three equations for the direct estimation of the airflow resistivity were chosen for the experiment reported in this work: (i) the Bies-Hansen equation [5]; (ii) Garai-Pompoli equation [6]; and the (iii)

* Corresponding author.
E-mail address: aihurrell1@sheffield.ac.uk (A.I. Hurrell).

http://dx.doi.org/10.1016/j.apacoust.2017.09.024
Received 19 May 2017; Received in revised form 11 August 2017; Accepted 27 September 2017
Available online 10 October 2017

Kozeny-Carman equation [7].

The airflow resistivity values predicted with these equations were then compared to those deduced via two mathematical models, which are able to invert the airflow resistivity of fibrous media from their acoustical properties. These models were: (i) the Miki model [8]; and the (ii) Padé approximation model [9].

2.1. Bies-Hansen equation

The Bies-Hansen equation [5] relates a material's airflow resistivity to its fibre diameter and bulk density:

$$\sigma d^2 \rho_m^{-K_1} = K_2. \tag{1}$$

In this equation, σ is the airflow resistivity [Pa s/m^2], ρ_m is the bulk density of the fibres [kg/m^3], d is the mean fibre diameter within the sample [m], and both K_1 and K_2 are dimensionless empirical constants – which have values of 1.53 and 3.18×10^{-9} for fibre glass materials, respectively. It should be noted that the work by Bies and Hansen [5] assumes that the materials have a uniform fibre diameter, which is less than 15μm, and that there is a negligible binder fibre content in the material sample.

2.2. Garai-Pompoli equation

Upon applying the Bies-Hansen equation to polyester fibre samples Garai and Pompoli found that the airflow resistivity values were grossly underestimated [6]. They surmised that this was as a result of polyester samples having larger fibre diameters than the fibreglass samples Bies-Hansen originally modelled, and so the constants fitted in the Bies-Hansen model were not sufficiently accurate to predict the actual value of airflow resistivity.

Garai and Pompoli proposed new values of the coefficients K_1 and K_2 in Eq. (1). Garai and Pompoli refer to their equation as the "new resistivity model (NRM)", which is [6]:

$$\sigma = A \rho_m^B, \tag{2}$$

where $A = K_2 d^{-2}$ and $B = K_1$. A and B are free parameters and so can be calculated for varying sample compositions to obtain the best fit. Garai and Pompoli reported that the values of $A = 25.989$ and $B = 1.404$ provided the best fit for polyester fibres, and so those were the values used in this experiment.

Garai and Pompoli also reported that from their analysis of four different types of polyester materials the binder fibre percentage did not seem to impact the precision of their equation, and that it was not affected by surface smoothing treatments [6]. Theoretically, this means that their model should be accurate for a broad range of the samples presented in this paper, some of which feature differing binder percentages.

2.3. Kozeny-Carman equation

The Kozeny-Carman equation originates from the 1930s and was originally employed to relate the porosity of granular media, for example soils and sands, to airflow resistivity [2,3]. This equation has subsequently been applied to estimate airflow resistivity of textiles, especially polymer fibres using the following relationship [7]:

$$\sigma = \frac{180\mu(1-\phi)^2}{d^2\phi^3} \tag{3}$$

μ is the dynamic viscosity, which is a constant derived from Poiseuille's equation of laminar flow for a liquid, and was assigned the value of 1.81×10^{-5} Pa s for this experiment, d is the particle size, which was assumed to be equivalent to the fibre diameter in Eq. (1), σ is the airflow resistivity and ϕ is the porosity, which was calculated from the ratio of bulk material density, ρ_m, to fibre density, ρ_f, via the following equation:

$$\phi = 1 - \frac{\rho_m}{\rho_f}. \tag{4}$$

From the above three equations it can be seen that the airflow resistivity of a sample is inversely dependent upon the fibre diameter squared, but the coefficients in these equations differ.

2.4. Miki model

The Miki Model was published by Miki in 1989 [8], as an improvement to the empirical model of Delany and Bazley [10]. Miki proposed some modifications to the Delany-Bazley model to yield a model that is more accurate and causal across a broader frequency range. According to the Miki model [7] the characteristic impedance of a porous medium can be calculated more accurately from:

$$z_b(f) = R(f) + iX(f), \tag{5}$$

$$R(f) = 1 + 0.070\left(\frac{f}{\sigma}\right)^{-0.632} \tag{6}$$

$$X(f) = 0.107\left(\frac{f}{\sigma}\right)^{-0.632}. \tag{7}$$

The wavenumber for sound propagation in porous media was also modified and given by the following equations:

$$k_b(f) = \alpha(f)i + \beta(f) \tag{8}$$

$$\alpha(f) = \frac{2\pi f}{c_0}\left[0.160\left(\frac{f}{\sigma}\right)^{-0.618}\right] \tag{9}$$

$$\beta(f) = \frac{2\pi f}{c_0}\left[1 + 0.109\left(\frac{f}{\sigma}\right)^{-0.618}\right]. \tag{10}$$

In the above equations f is the frequency of the sound wave (Hz), and c_0 is the speed of sound in air (m/s) and $i = \sqrt{-1}$.

2.5. Padé approximation model (PadéNUP)

The Padé approximation model was proposed by Horoshenkov et al. [9] and it makes use of the Padé approximant theory to approximate the viscosity correction function in the expressions for the characteristic impedance and wavenumber in a porous medium with non-uniform pores:

$$z_b(\omega) = \sqrt{\widetilde{\rho}_b(\omega)/\widetilde{C}_b(\omega)} \text{ and } k_b(\omega) = \omega\sqrt{\widetilde{\rho}_b(\omega)\widetilde{C}_b(\omega)}, \tag{11}$$

where $\widetilde{C}_b(\omega) = 1/\widetilde{K}(\omega)$ is the bulk complex compressibility of air in the material pores, $\widetilde{K}(\omega)$ is the dynamic bulk modulus of the air in the material pores and $\widetilde{\rho}_b(\omega)$ is the dynamic density of the air in the material pores and $\omega = 2\pi f$ is the circular frequency.

The Padé approximation model makes use of approximations for the dynamic density (Eq. (12)), and one for approximating the complex compressibility (Eq. (14)). According to this model the dynamic density can be expressed as:

$$\widetilde{\rho}_x(\epsilon_\rho) = 1 + \epsilon_\rho^{-2}\,\widetilde{F}_\rho(\epsilon_p), \tag{12}$$

where the viscosity correction function is given by a Padé approximant:

$$\widetilde{F}_\rho(\epsilon_p) = \frac{1 + \theta_{\rho,3}\,\epsilon_\rho + \theta_{\rho,1}\,\epsilon_\rho}{1 + \theta_{\rho,3}\,\epsilon_\rho}, \tag{13}$$

with $\epsilon_\rho = \sqrt{-i\omega\rho_0/\sigma_x}$. In the above Padé approximation, the coefficients $\theta_{\rho,1} = 1/3$, $\theta_{\rho,2} = \sqrt{1/2}\,e^{1/2(\sigma_s \log 2)^2}$, $\theta_{\rho,3} = \theta_{\rho,1}/\theta_{\rho,2}$ are real and positive numbers.

Similarly, the complex compressibility is:

$$\widetilde{C}_x(\epsilon_c) = \frac{1}{\gamma P_0}\left(\gamma - \frac{\gamma - 1}{1 + \epsilon_c^{-2}\,\widetilde{F}_c(\epsilon_c)}\right), \tag{14}$$

where

$$\widetilde{F}_c(\epsilon_c) = \frac{1 + \theta_{c,3}\,\epsilon_c + \theta_{c,1}\,\epsilon_c}{1 + \theta_{c,3}\,\epsilon_c}. \tag{15}$$

The coefficients in (15) are $\theta_{c,3} = \theta_{c,1}/\theta_{c,2}$, $\theta_{c,2} = \sqrt{1/2}\,e^{3/2(\sigma_s \log 2)^2}$, $\theta_{c,1} = 1/3$ and the frequency dependent parameter is $\epsilon_c = \sqrt{(-i\omega\rho_0 N_{Pr}/\sigma_x')}$. In the above equations σ_x is the air flow resistivity of a single pore and σ_x' is the thermal flow resistivity in the pore which physical meaning is detailed in Ref. [9]. Here N_{Pr} is the Prandtl number, γ is the ratio of specific heats and σ_s is the standard deviation in the log-normal distribution in the pore size. For fibrous media with a relatively high porosity $\sigma_s \approx 0$.

These equations are for single pore materials, and so for bulk materials with a plurality of pores some of the parameters must be changed so that the effective flow resistivity is expressed as:

$$\sigma = \frac{\sigma_x \alpha_\infty}{\phi}, \tag{16}$$

the effective bulk density:

$$\widetilde{\rho}_b = \frac{\alpha_\infty}{\phi}\widetilde{\rho}_x \tag{17}$$

with

$$\epsilon_\rho = \sqrt{\frac{-i\omega\alpha_\infty\rho_0}{\phi\sigma}}. \tag{18}$$

$\widetilde{C}_x$ for a single pore must also be replaced with its bulk equivalent:

$$\widetilde{C}_b = \phi \cdot \widetilde{C}_x, \tag{19}$$

where

$$\epsilon_c = \sqrt{\frac{-i\omega\alpha_\infty\rho_0}{\phi\sigma'}} \tag{20}$$

and

$$\sigma' = \frac{\sigma_x' \cdot \alpha_\infty}{\phi}. \tag{21}$$

2.6. Parameter inversion process

The equations for the characteristic impedance and wavenumber can be used to predict the surface impedance of a hard-backed porous specimen of thickness, h

$$z(f) = z_b \coth(-ik_b h). \tag{22}$$

In this case, the flow resistivity of the fibrous material specimen can be inverted by finding the minimum of the following equation

$$F(x) = \sum_{n=1}^{N} \{z^{exp}(f_n) - z^{th}(f_n,\sigma)\} \rightarrow min, \tag{23}$$

where $z^{exp}(f_n)$ is the measured surface impedance spectrum, $z^{th}(f_n,\sigma)$ is the predicted surface impedance spectrum, f_n the array of frequencies at which the impedance data were measured.

The porosity, ϕ, of the fibrous samples was measured independently and it was used in the inversion process. It is easy to show that for this type of fibrous media of low density and high porosity the tortuosity α_∞ is close to unity within 1–3%. In this case the Miki and Padé approximation models become relatively independent of this parameter. Therefore, in the inversion process this parameter was set to one to enhance the convergence of computation. In this work, the minimisation problem was solved via a Nelder-Mead optimisation algorithm [11].

Table 1
Fibrous material compositions of the eight samples used in the reported experiments. The percentages show the relative composition of fibres with a particular denier value.

Sample	Composition
Sample 1	25% 4d PET, 55% 6d PET, 20% 6d PET
Sample 2	28% 4d PET binder, 52% 4d, 20% 1.7d PET
Sample 3	10% 4d PET, 75% rags, 12% 15d, 3% 4d
Sample 4	15% 4d PET, 50% cotton, 17.5% 6d PET, 17.5% binder
Sample 5	75% 6.7d PET, 25% binder
Sample 6	75% 1.5d PET, 25% binder
Sample 7	75% 1.5d PET, 25% binder
Sample 8	40% 1.5d PET, 35% 15d PET, 25% binder

Table 2
Key material data for the eleven fibrous samples used in the reported experiments.

Sample	Fibre diameter (μm)	Fibre density (kg/m^3)	Bulk density (kg/m^3)	Porosity	Thickness (mm)
Sample 1	23.66	1381	60.35	0.96 ± 0.0010	34 ± 0.5
Sample 2	18.83	1379	32.68	0.98 ± 0.0007	46 ± 0.4
Sample 3	N/A	1378	43.82	0.97 ± 0.0009	45 ± 0.3
Sample 4	N/A	1383	27.94	0.98 ± 0.0005	50 ± 0.2
Sample 5	24.71	1383	21.71	0.98 ± 0.0010	47 ± 0.3
Sample 6	14.36	1379	24.68	0.98 ± 0.0005	42 ± 0.3
Sample 7	14.36	1379	38.47	0.97 ± 0.0004	43 ± 0.5
Sample 8	23.74	1383	17.57	0.99 ± 0.0003	54 ± 0.4

3. Experimental methodology

All material samples used within this work were provided by John Cotton Group Ltd. Tables 1 and 2 show the composition of these materials and some of their material parameters. In these tables, the nomenclature “PET” refers to polyester, “d” refers to denier, and “binder” stands for a polyester binder fibre. Images of the samples used can be found in Appendix A.

Table 1 presents the fibre diameter in terms of the denier value. This value was converted to the SI unit using the following relation

$$d = 11.89 \times \sqrt{\frac{d_{den}}{\rho_f}}, \tag{24}$$

where d is the fibre diameter in metres, d_{den} is the denier, and ρ_f is the fibre density in kg/m^3. The fibre density was calculated from porosity and bulk density measurements, its values for all the material specimens is given in Table 2. This table also presents the mean fibre diameter in the SI units. The fibre composition was taken into account to generate an average fibre diameter which was based on the weighted proportion of each fibre in the blend. The fibre diameter of the samples Sample 3 and Sample 4 was unknown, as the authors were unable to measure reliably the fibre diameter values. This is because the samples were made from recycled materials and so no denier value was provided. We were also unable to obtain a value for the fibre diameter through the measurement of the samples as too great a variety of diameters were found to be able to estimate it accurately or to measure its value directly.

Calculations of the material characteristics such as bulk density, porosity and thickness were all done in the Jonas Lab at the University of Sheffield. Bulk density was calculated from a measure of volume and sample weight, as weighed on a Kern KB10000-1N scale. The specimen thickness was measured using digital callipers for each individual sample. In each case the thickness values have been rounded to the nearest millimetre to minimise any inaccuracies caused by partial compression of the samples by the callipers. The porosity of the samples was measured using an in-house manufactured porosimeter which works on the Boyles law principle detailed in Ref. [12]. Each sample was measured three separate times, and the results averaged to give the

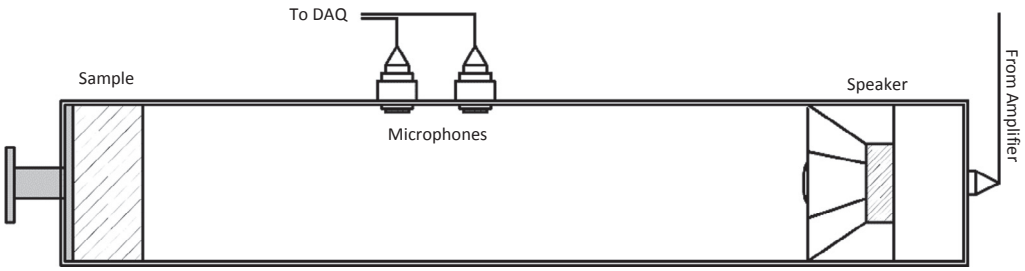

Fig. 1. Two-microphone acoustic impedance tube schematic.

porosity value used in the models (see Table 2). The porosimeter has an accuracy of 1%, as assessed via comparisons of calibration samples analysed through alternative methods at various institutions [13]. Given the accuracy of the porosimeter, any deviations there are likely to be negligible and would have minimal effect on the evaluated values of airflow resistivity. As an example, if we change the porosity value of Sample 1 to 0.98, from 0.96 (a value much greater than the differences encountered during the measurement, see Table 2), then the value of airflow resistivity, as evaluated by the Padé approximation model, changes from 27242 Pa s/m^2 from its original value of 27243 Pa s/m^2 which is well below the experimental error. A similar change would occur if the Miki model is adopted for the flow resistivity inversion.

The material specimens were run in triplicate, in the form of 100 mm cylinders prepared using a special hole-cutter. The surface impedance of these material specimens was measured in accordance with the ISO 10534-2 [4] to measure the surface impedance, using a 100 mm impedance tube manufactured by Materiacustica [14]. Fig. 1 schematically illustrates the two microphone impedance tube set-up that was used in this work.

The measured values for surface impedance and other parameters were then substituted into Eq. (7) to solve the minimisation problem, utilising a standard MATLAB minimisation subroutine 'fminsearchbnd ()' [15]. The subroutine was applied in the frequency range of 200–1500 Hz. The lower boundary was chosen to avoid any inaccuracies caused by phase mismatch or structural vibrations in the acoustic impedance tube. In both cases, root mean squared errors were generated from the absolute values of the measured impedance. Fig. 2 presents the measured and predicted (through the minimisation algorithm, Eq. (23)) real and imaginary parts of the surface impedance for a material sample of Sample 1. The root mean square error between the measured and predicted value of the normalised surface impedance for all material samples was below 9.6%, and had an average of 1.6% for all samples.

The airflow resistivity was also measured directly using an AFD AcoustiFlow 300, supplied by Akustik Forschung Dresden, and used alongside their AFD 311 software package [16]. The AcoustiFlow is able to determine the airflow resistivity of materials with open porosity based on a direct-airflow method, as outlined in the ISO 9053 [17]. This method measures the pressure drop at the specimen as a function of the volume airflow. Specimens for the blended fibre samples were inserted into a 100 mm sample holder, and analysed at a temperature of 21.0 °C ± 0.5. Five specimens for each sample were tested and the airflow resistivity value was taken as an average of these five specimens. No further processing or calculations were applied. In an effort to ensure that the variation of thicknesses between samples did not significantly affect the accuracy of the measured results, each material was tested ten times with a single thickness and ten times with a double thickness. The relative standard deviation in the flow resistivity across all twenty tests was 3.60%, and as such it was concluded that thickness does not have a significant effect. The mean numerical values of the flow resistivity for each material specimen studied in this work are provided in Appendix B and include the measurement errors.

4. Results

Fig. 3 presents a summary of the measured, inverted and predicted flow resistivity data for all fibrous samples studied in this work. Table 3 presents the average numerical values of the flow resistivities plotted in Fig. 3. Table 4 presents the percentage differences between a predicted/inverted value of the flow resistivity and the measured value. There is generally limited agreement between the flow resistivity predicted by the three equations (Eqs. (1)–(3)) which make use of fibre diameter and material density data. The maximum difference of 88% is observed in the case of the Bies-Hansen equation applied to Sample 8 material data. The Bies-Hansen equation consistently underestimates the airflow resistivity when compared to the results from the Garai-Pompoli and Kozeny-Carman equations. The Garai-Pompoli equation tends to overpredict the flow resistivity except in the case of Sample 8 material. The Kozeny-Carman equation tends to underpredict the flow resistivity except in the case of Sample 1 material. The maximum difference of −75% is between the flow resistivity predicted by the Kozeny-Carman equation and the measured value for Sample 8 material. The maximum difference of 59% is between the flow resistivity predicted by the Garai-Pompoli equation and the measured value for Sample 2 material.

The differences between the inverted and measured values of the flow resistivity are smaller than those between the predicted and measured. Here the maximum difference of 42% is between the flow resistivity inverted with the Padé approximation (PadéNUP) and that measured for Sample 6. The flow resistivity values inverted with the Miki model is much closer to their measured equivalents. Here the maximum difference of 15% is for the case of Sample 4 material. For the other materials, the differences between the value of the flow resistivity inverted with the Miki model and its measured value are much less. The maximum mean error produced by the Miki model occurs during the inversions of Sample 3, with a value of 8.8%. The maximum mean error

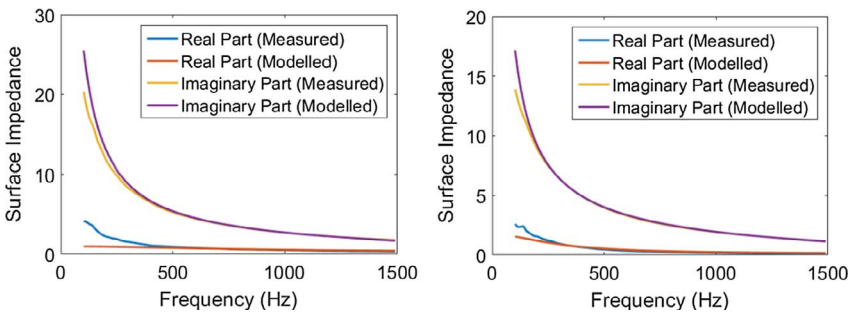

Fig. 2. Examples of the measured and predicted values of normalised surface impedance (–) for the Miki (left) and Padé approximation (right) models for the blended samples. These graphs are results from testing the material Sample 1, at single thickness of 15.07 mm.

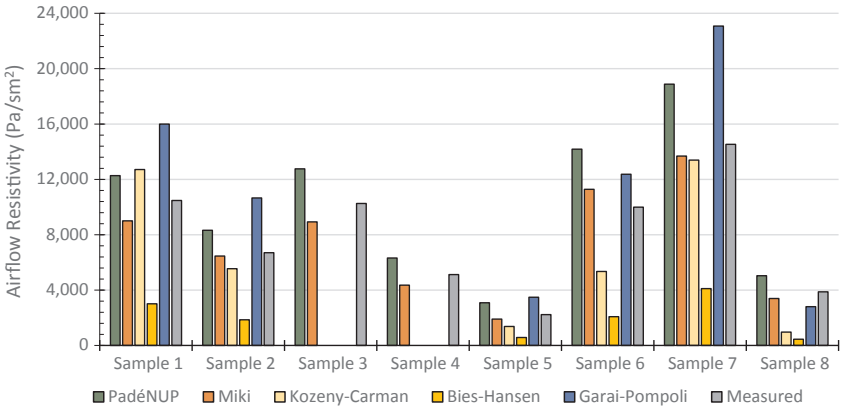

Fig. 3. A summary of the measured, inverted and predicted flow resistivity values for the material samples.

Table 3
Comparison of the measured, inverted and predicted airflow resistivity values for the blended fibre samples, rounded to the nearest ten.

	PadéNUP	Miki	Kozeny-Carman	Bies-Hansen	Garai-Pompoli	Measured
Sample	Flow Resistivity (Pa s/m^2)					
Sample 1	12,270	9010	12,710	3010	16,000	10,480 ± 377
Sample 2	8330	6470	5540	1860	10,660	6700 ± 256
Sample 3	12,760	8930	N/A	N/A	N/A	10,260 ± 180
Sample 4	6320	4360	N/A	N/A	N/A	5130 ± 36
Sample 5	3080	1910	1380	580	3490	2230 ± 109
Sample 6	14,180	11,280	5350	2080	12,370	9990 ± 67
Sample 7	18,880	13,690	13,390	4110	23,080	14,530 ± 31
Sample 8	5040	3400	970	450	2810	3880 ± 54

produced by the Padé approximation model occurs during the inversions of Sample 1, with a value of 9.3%.

For this work, the authors consider any result within an error of 10% to be considered accurate for this kind of analysis, as the value of bulk density for a sample can vary by a similar amount due to several uncertainties during measurement due to fibre compression, fibre density, and any inaccuracies or noise present during the acquisition of the acoustical data which may have given slightly erroneous data.

From these results, it could be concluded that the Miki model is superior in terms of the flow resistivity inversion when compared to the Padé approximation model, Bies-Hansen, Kozeny-Carman and Garai-Pompoli equations. It could also be said that the Bies-Hansen, Kozeny-Carman and Garai-Pompoli equations have a few significant drawbacks such as the requirement to know several material parameters in advance of the experiment. Some parameters, e.g. fibre diameter and its distribution, can be difficult to measure or to predict. Conversely, the Miki and Padé approximation models can be run, and to a good accuracy, without the knowledge of any parameter other than the material's thickness.

Table 4
Differences between airflow resistivity results for each model and equation against experimentally obtained values from the AcoustiFlow 300. Negative values reflect results lower than measured, and vice versa.

	Percentage difference (%) vs measured FR values				
Sample	PadéNUP	Miki	Kozeny-Carman	Bies-Hansen	Garai-Pompoli
Sample 1	17	−14	21	−71	53
Sample 2	24	−4	−17	−72	59
Sample 3	24	−13	N/A	N/A	N/A
Sample 4	23	−15	N/A	N/A	N/A
Sample 5	38	−14	−38	−74	57
Sample 6	42	13	−47	−79	24
Sample 7	30	−6	−8	−72	59
Sample 8	30	−12	−75	−88	−28

5. Conclusions

The scope of this paper was to review the performance of five commonly used and widely accepted equations and models for the prediction or inversion of the flow resistivity of nonwoven fibrous materials consisting of a blend of fibre diameters. Eight material samples with the measured flow resistivities in the range of 2229 and 14,530 Pa s/m^2 have been studied. The results suggest that the value of the flow resistivity inverted with either Padé approximation or Miki model is more accurate than that predicted using Bies-Hansen, Garai-Pompoli or Kozeny-Carman equations. In particular, the Miki model enables the inversion of flow resistivity of this type of fibrous media from measured surface impedance data with an accuracy of better than 15%. The Padé approximation model enables the inversion of flow resistivity with the accuracy of better than 42%. The latter error is likely related to the fact that the Miki model requires fewer parameters so that it can be more stable in the parameter inversion process. The pore structure of fibrous media with high porosity is relatively uniform so that the convergence of the Miki model for this type of media is better than that of the pore distribution model based on the Padé approximation. The proposed parameter inversion is a straightforward process which can be used to understand better the relationship between the material density and fibre diameter distribution and the resultant value of the flow resistivity of a porous medium. The flow resistivity inversion based on the Miki or Padé approximation model is attractive as it can be run without the prior knowledge of any intrinsic material property other than the material's thickness.

Among the three prediction-based equations for flow resistivity, the Garai-Pompoli and Kozeny-Carman models appear more accurate than that by Bies and Hansen. A suspected reason for a relatively limited performance of the three equations is that these equations are only valid for a uniform fibre diameter media. In the instance of the blended fibres studied in this paper the coefficients in the three equations are no longer valid and need to account for the distribution in the fibre diameter. This work suggests that new equations are required to relate the

flow resistivity of blended fibrous media to the material density and fibre diameter distribution.

Acknowledgments

The authors would like to thank John Cotton Group Ltd for supplying the samples. We would also like to thank Leslie Morton for his help throughout the sample preparation and characterisation stages. The authors are grateful for the financial support of this work by the EPSRC-sponsored Centre for Doctoral Training in Polymers, Soft Matter and Colloids at Sheffield.

Appendix A. Images of the samples used within this experiment, taken from the 'top' down and side-on

See Figs. A1–A4.

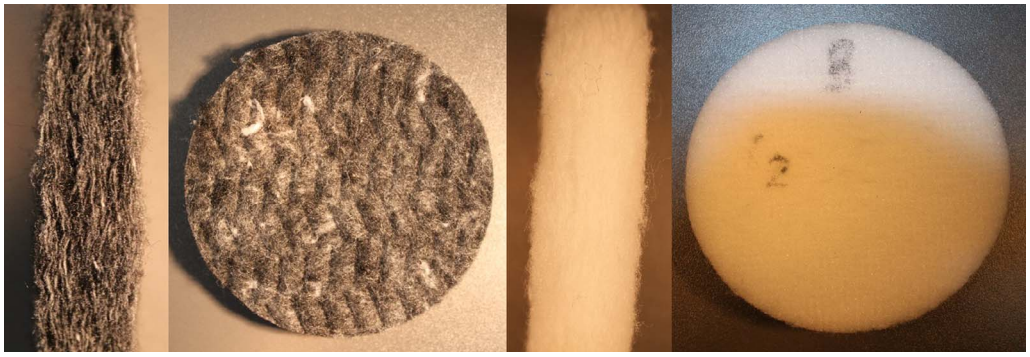

Fig. A1. Sample 1, left, and Sample 2, right.

Fig. A2. Sample 3, left, and Sample 4, right.

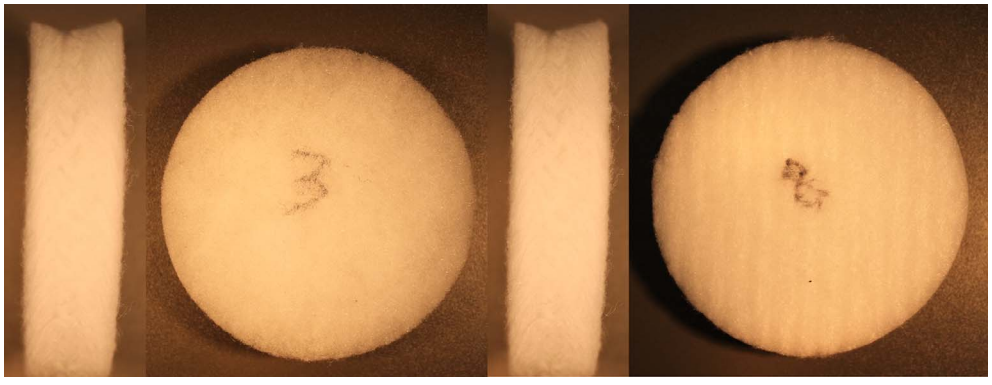

Fig. A3. 3 Sample 5, left, and Sample 6, right.

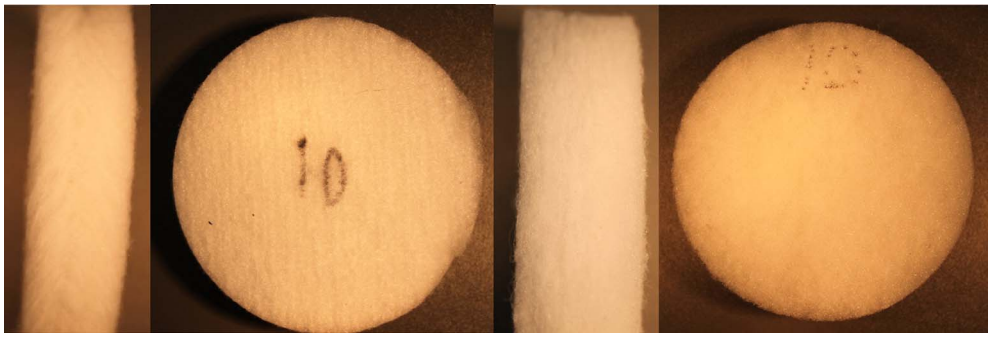

Fig. A4. Sample 7, left, and Sample 8, right.

Appendix B. The measured airflow resistivity values

See Table B1.

Table B1
Measured flow resistivity (FR) values for Sample 1.

Measurement	σ in Pa s/m^2
Sample 1 Double (1)	9968
Sample 1 Double (2)	10,130
Sample 1 Double (3)	10,214
Sample 1 Double (4)	10,110
Sample 1 Double (5)	10,156
Sample 1 Double (6)	10,185
Sample 1 Double (7)	10,127
Sample 1 Double (8)	10,170
Sample 1 Double (9)	10,223
Sample 1 Double (10)	10,151
Sample 1 Single (1)	10,696
Sample 1 Single (2)	10,419
Sample 1 Single (3)	10,742
Sample 1 Single (4)	10,937
Sample 1 Single (5)	10,789
Sample 1 Single (6)	10,998
Sample 1 Single (7)	10,608
Sample 1 Single (8)	10,966
Sample 1 Single (9)	11,162
Sample 1 Single (10)	10,807
Average	10,478
Standard deviation	377

It should be noted that ‘single’ and ‘double’ refer to the thickness of the sample used in the AcoustiFlow 300 device. The bracketed numbers are the test numbers.

See Tables B2–B8.

Table B2
Measured FR values for Sample 2.

Measurement	σ in Pa s/m^2
Sample 2 (1)	6971
Sample 2 (2)	6490
Sample 2 (3)	6542
Sample 2 (4)	6513
Sample 2 (5)	6990
Average	6701
Standard deviation	256

Table B3
Measured FR values for Sample 3.

Measurement	σ in Pa s/m^2
Sample 3 (1)	10,578
Sample 3 (2)	10,148
Sample 3 (3)	10,209
Sample 3 (4)	10,183
Sample 3 (5)	10,176
Average	10,259
Standard deviation	180

Table B4
Measured FR values for Sample 4.

Measurement	σ in Pa s/m^2
Sample 4 (1)	5107
Sample 4 (2)	5172
Sample 4 (3)	5111
Sample 4 (4)	5157
Sample 4 (5)	5087
Average	5127
Standard deviation	36

Table B5
Measured FR values for Sample 5.

Measurement	σ in Pa s/m^2
Sample 5 (1)	2179
Sample 5 (2)	2417
Sample 5 (3)	2220
Sample 5 (4)	2146
Sample 5 (5)	2182
Average	2229
109	

Table B6
Measured FR values for Sample 6.

Measurement	σ in Pa s/m^2
Sample 6 (1)	9889
Sample 6 (2)	10,043
Sample 6 (3)	9964
Sample 6 (4)	10,020
Sample 6 (5)	10,046
Average	9992
Standard deviation	67

Table B7
Measured FR values for Sample 7.

Measurement	σ in Pa s/m^2
Sample 7 (1)	14,501
Sample 7 (2)	14,493
Sample 7 (3)	14,560
Sample 7 (4)	14,550
Sample 7 (5)	14,545
Average	14,530
Standard deviation	31

Table B8
Measured FR values for Sample 8.

Measurement	r in Pa s/m^2
Sample 8 (1)	3854
Sample 8 (2)	3925
Sample 8 (3)	3887
Sample 8 (4)	3923
Sample 8 (5)	3795
Average	3877
Standard deviation	54

References

[1] Nichols Jr. RH. Flow-resistance characteristics of fibrous acoustical materials. J Acoust Soc Am 1947;19(5):866–71.
[2] Kozeny J. Über kapillare Leitung des Wasser sim Boden; (Aufsteig, Versickerung und Anwendung auf die Bewässering). Hölder-Pichler-Tempsky; 1927.
[3] Carman PC. Fluid flow through granular beds. Trans Instn Chem Engrs 1937;15:S32–47.
[4] ISO10534-2:1998. Determination of sound absorption coefficient and impedance in impedance tubes, Part 2: Transfer-function method international organization for standardization, Geneva, Switzerland; 1998.
[5] Bies DA, Hansen CH. Flow resistance information for acoustical design. Appl Acoust 1980;13(5):357–91.
[6] Garai M, Pompoli F. A simple empirical model of polyester fibre materials for acoustical applications. J Appl Acoust 2005;66:1383–98.
[7] Pelegrinis M, Horoshenkov KV, Burnett A. An application of Kozeny – Carman flow resistivity model to predict the acoustical properties of polyester fibre. J Appl Acoust 2016;111:1–4.
[8] Miki Y. Acoustical properties of porous materials – modifications of Delany-Bazley models. J Acoust Soc Jpn 1990;11(1):19–24.
[9] Horoshenkov KV, Groby J-P, Dazel O. Asymptotic limits of some models for sound propagation in porous media and the assignment of the pore characteristic lengths. J Acoust Soc Am 2016;139:2436–74.
[10] Delany ME, Bazley EN. Acoustical properties of fibrous absorbent materials. Appl Acoust 1970;3:105–16.
[11] Nelder JA, Mead R. A simplex method for function minimization. Comput J 1965;7(4):308–13.
[12] Leclaire P, Umnova O, Horoshenkov KV. Porosity measurement by comparison of air volumes. Rev Sci Instrum 2003;74(3):1366–70.
[13] Horoshenkov KV, Khan A, Bécot F-X, Jaouen L, Sgard F, Renault A, et al. Reproducibility experiments on measuring acoustical properties of rigid-frame porous media (round-robin test). J Acoust Soc Am 2007;122(1):345–53.
[14] Materiacustica SRL. < http://www.materiacustica.it/mat_Prodotti_3Mics.html > [accessed on 20/09/2016].
[15] MatWorks. < http://uk.mathworks.com/matlabcentral/fileexchange/8277-fminsearchbnd–fminsearchcon > [last visited on 22/09/2016].
[16] Akustik Forschung Dresden. < http://www.akustikforschung.de/en/produkte/messgerate/stromungswiderstandsmessgerat-afd-300-acoustiflow/ > [last visited on 18/04/2017].
[17] ISO9053:1991. < https://www.iso.org/standard/16622.html > [last visited on 18/04/2017].